Electronic Supplementary Material (ESI) for CrystEngComm.

Electronic Supplementary Information (ESI) for A Heterometallic Nano Sized Tube $\{Fe[(CN)_6]_2[Co(L_{N3O2})]_3\}_n$ and Two of Its Lamellar Polymorphous Isomers

Feng Pan[*ab], Song Gao[*a] and Hui-Zhou Liu[*b]

[a]Beijing National Laboratory for Molecular Sciences, State Key Lab of Rare Earth Materials Chemistry and Applications, College of Chemistry and Molecular Engineering, Peking University, Beijing 100871, P. R. China

[b] Key Laboratory of Green Process and Engineering, State Key Laboratory of Biochemical Engineering, Institute of Process Engineering, Chinese Academy of Sciences, Beijing 100190, PR China

pfeng@ipe.ac.cn

gaosong@pku.edu.cn

hzliu@ipe.ac.cn

S1. Experimental Details

All staring materials were commercially available, reagent grade, and used as purchased. All preparations and manipulations were performed under aerobic conditions except for specified. Elementary analysis of C, H, and N were carried out on an Elementary Vario EL analyzer.

WARNING: Cyanides are extremely toxic perchlorates are explosive and should be handled with caution.

1. Synthesis of precursor compound $[Co(L_{N3O2})](ClO_4)_2 \cdot xSolvent$

1.63 g 2, 6-diethanonne pyridine was dissolved in 50 mL methanol, resulted solution was added 3.56 g $CoClO_4 \cdot 6H_2O$ and 0.25 g $Na_2S_2O_3$, and heated it to 50 ℃ under a nitrogen protection, then 50 mL methanol solution of 2, 2'-(ethane-1,2-diylbis(oxy)) diethanamine (1.48 g) was added into the former solution at 50 ℃, the reaction continued in another 18 hours in reflux condition. Dark red filtrate was obtained, evaporate it until a mount of dark red solid separated out, filtrated it, collected resulted solid and recrystallize it with a mixture of ether and methanol (ether : methanol/10 : 1) with a yield about 45%.

2. Synthesis of compounds crystal suitable for X-ray diffraction analysis

One arm of H-shaped tube was added 6.0 mL methanol solution containing 0.120 g $[Co(L_{N3O2})](ClO_4)_2$, the other arm was added 6.0 mL water solution containing 0.008 g $K_3[Fe(CN)_6]$, then carefully connect them with iso-propanol. After a half month, stick shaped brown crystals of compound **1** ($Fe[(CN)_6]_4[Co(L_{N3O2})]_6 \cdot 19H_2O$) were observed on the wall of $K_3[Fe(CN)_6]$ side, which are suitable of X-ray diffraction. Anal. Calc. for $Co_{24}Fe_{16}C_{456}H_{516}N_{168}O_{126}$ (%): C:43.21; H: 4.10; N: 18.57. Found: C:43.19; H:4.05; N: 18.65. IR stretching cyanide: 2117 cm^{-1}(strong), 2072 cm^{-1}(week).

The single crystal of compound **2** was obtained using a test tube. 4 mL aqua solution of 0.090 g $[Co(L_{N3O2})](ClO_4)_2$ was placed on the bottom of the tube, then layered by 2mL water, on the water layer added 6 mL aqua solution containing 0.050 g $K_3[Fe(CN)_6]$. After a half month, brick shaped crystal of compound **2** ($Fe[(CN)_6]_2[Co(L_{N3O2})]_3 \cdot 14H_2O \cdot 2CH_4O$) has separated out on the wall, the color is brown. Anal. Calc. For $Co_{12}Fe_8C_{236}H_{252}O_{96}N_{84}$ (%): C:40.76; H: 3.65; N: 16.92. Found: C:39.28; H:3.39; N: 17.10. IR stretching cyanide: 2117 cm^{-1}(strong).

Compound **3** ($Fe[(CN)_6]_2[Co(L_{N3O2})]_3 \cdot 6H_2O$) was obtained with a similar method as compound **1**, a H-shaped tube was used, one arm was also added 6.0 mL methanol solution containing 0.12 g $[Co(L_{N3O2})](ClO_4)_2$, but the other arm was added 6.0 mL water solution containing 0.050 g $K_3[Fe(CN)_6]$, and the two parts was connected by water very carefully. After a month, long block shaped crystal was observed on the $K_3[Fe(CN)_6]$ side. Anal. Calc. for $Co_{12}Fe_8C_{231}H_{264}N_{84}O_{51}$ (%): C:44.84; H: 4.30; N: 19.02. Found: C:44.97; H:4.51; N: 18.92. IR stretching cyanide: 2129 cm^{-1}(strong), 2074 cm^{-1}(week).

3. Metal content measurement: The crystal samples were weighed and dissolve in 2 M HNO_3, and then diluted with deionized water in volumetric flasks. The concentrations of the metals in the obtained aqueous were measured using inductively coupled plasma-optical emission spectrometer (ICP-OES) (PerkinElmer, USA). The metal mass fractions in crystal sample are calculated: compound 1: Fe 7.3% Co 12%; compound 2: Fe 6.5% Co 9.9%; compound 3 Fe 7.1% Co 12%.

4. X-ray Crystallographic Study: Crystallographic Data Collection and Structure Determination

The diffraction data collections of **1** and **3** were made at 293 K, **2** at 198 K, on a Nonius−CCD diffractometer. The structures were solved by the direct method (SHELXS-97) and refined by

full-matrix least squares (SHELXL-97) on F^2. Anisotropic thermal parameters were used for the non-hydrogen atoms. Hydrogen atoms were added geometrically, and a riding model was used to refine them. Weighted *R* factors (*wR*) and all of the goodness-of-fit (*S*) values were based on F^2; conventional *R* factors (*R*) were based on *F*, with *F* set to zero for negative F^2.

It was necessary to constrain or restrain a large number of bond lengths and angles in the structures of **1** and **3** in order to get stable refinements and chemically reasonable models. Some carbon and nitrogen atoms were restrained to have similar ADP's as their neighbors with isor, simu and delu command in the refinement for the compounds due to the large atomic displacement parameters for many atoms.

Disordered water molecules in the unit cells of compounds **1** and **3** were treated as a diffuse contribution to the overall scattering without specific atom positions by SQUEEZE/PLATON[1].

5. Physical measurements

Samples for physical measurements were all collected carefully from first batch of single crystal with fine distinguishing shape, the purities were proved by PXRD patterns shown in Figure S8. However it is beyond our ability to collect enough samples for accurate TGA and BET measurements.

FTIR spectra were recorded using pure samples in the range of 4000 to 650 cm^{-1} on a Nicolet Magna 750 FT/IR spectrometer. Dc and ac magnetic data were obtained on a Quantum Design MPMS5XL SQUID system. Diamagnetic corrections were estimated using Pascal constants[2], and background correction by experimental measurement on sample holders.

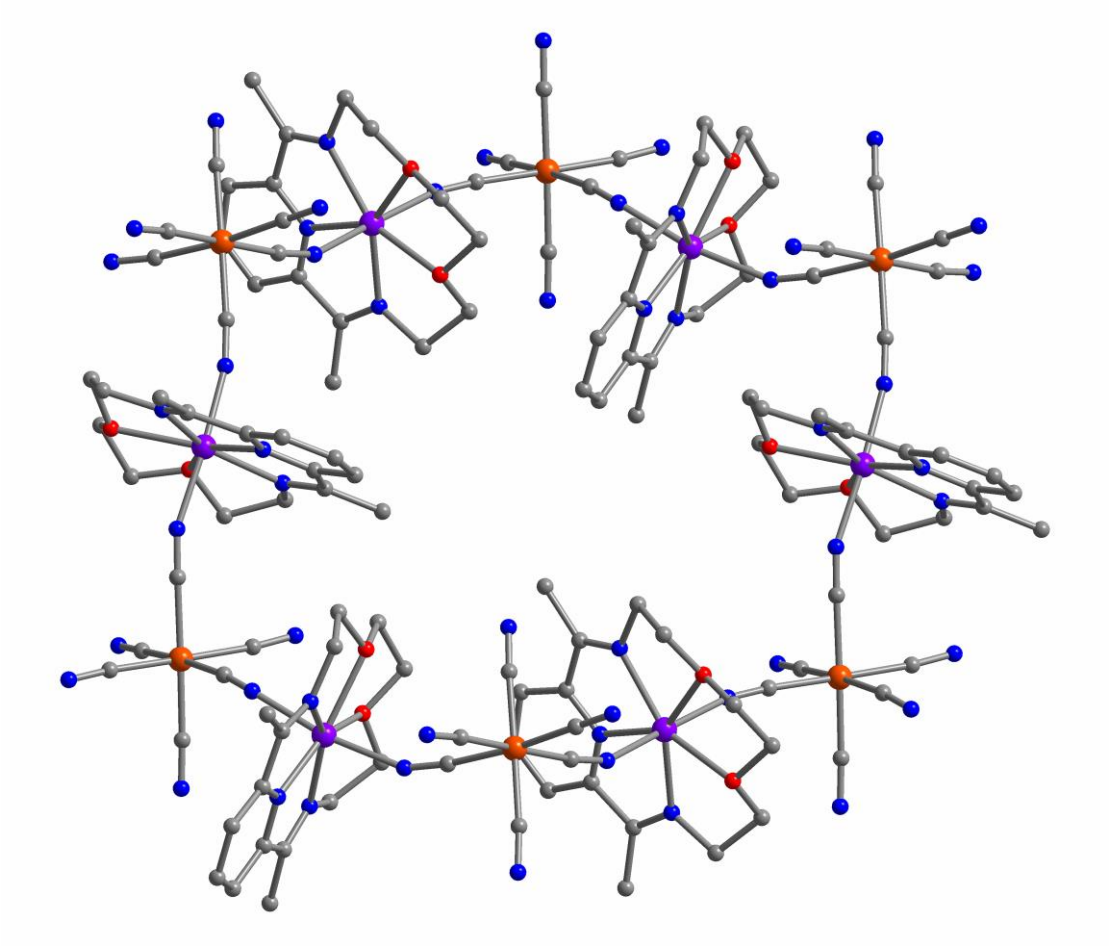

Figure S2. Twelve-member Fe-Co alternating ring as the structural unit of these three compounds. Orange and purple atoms are symbolizing iron and cobalt respectively.

Table S3. Summary of Crystallographic Data for Compounds

	1	2	3
formula	Co6Fe4C114 H164N42O31	Co3Fe2C59 H99 N21O22	Co3Fe2C57 H75N21O12
Mr [g/mol]	3195.85	1743.08	1534.87
crystal system	Monoclinic	Monoclinic	Monoclinic
space	P 21/c	C 2/c	P 21/n
a [Å]	17.276(4)	26.362(5)	10.187 (2)
b [Å]	29.697(6)	16.670 (3)	42.792(9)
c [Å]	31.436(6)	19.521(4)	17.083(3)
α [°]	90	90	90
β [°]	98.50(3)	108.29 (3)	101.50(3)
γ [°]	90	90	90
V [Å3]	15951(6)	8145(3)	7297(3)
Z	4	4	4
ρcalcd [mgcm–3]	1.331	1.421	1.397
F(000)	6624	3636	3172
crystal size [mm]	0.95 ×0.35 ×0.35	0.42 ×0.25 ×0.20	0.52 ×0.23 ×0.15
θlimit [°]	3.48–25.00	3.64−25.00	3.40−25.00
collected refln	50432	42786	88271
unique refln	26036	7612	12556
Rint	0.0763	0.1437	0.1339
no. of params	26036 /2758 /1765	7612/6 /494	12556/681 /921
GooF	1.064	1.203	0.934
R1a	0.0737	0.0638	0.0940
wR2b	0.1820	0.1595	0.2726

[a] $R_1 = \Sigma||F_0|-|F_c||/\Sigma|F_0|$; [b] $wR_2 = \Sigma[w(F_0^2-F_c^2)^2]/\ \Sigma[w(F_0^2)^2]^{1/2}$

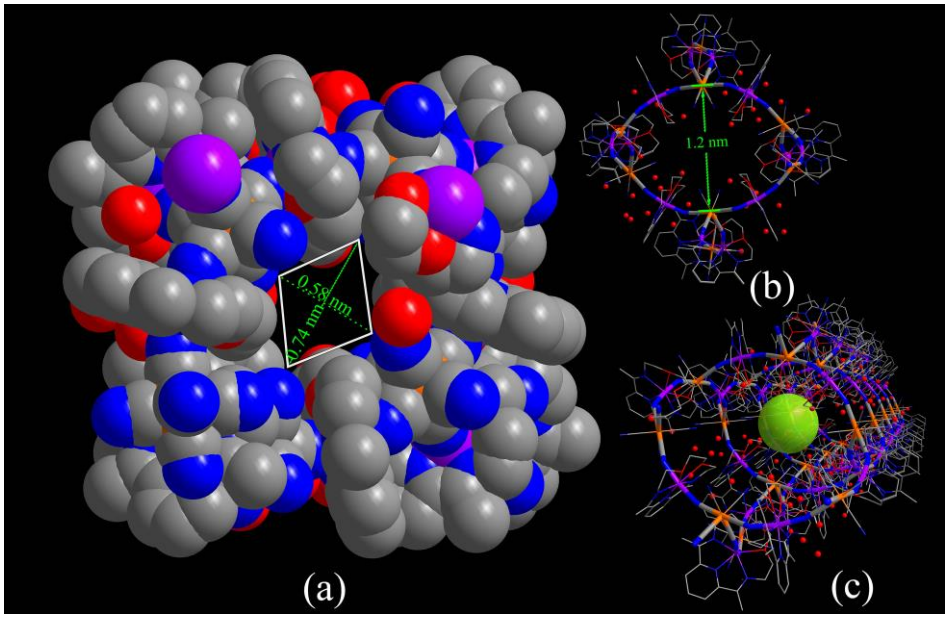

Figure S4. Some other structural graphs of **1** (a) Filling diagram with Vander Waals radii，and the rhombus tunnel with two diagonals measured 0.74 nm and 0.58 nm. (b) The metal framework with a diameter of 1.2 nm. (c) 1 D tunnel containable of the dummy atom with the diameter of 0.6 nm.

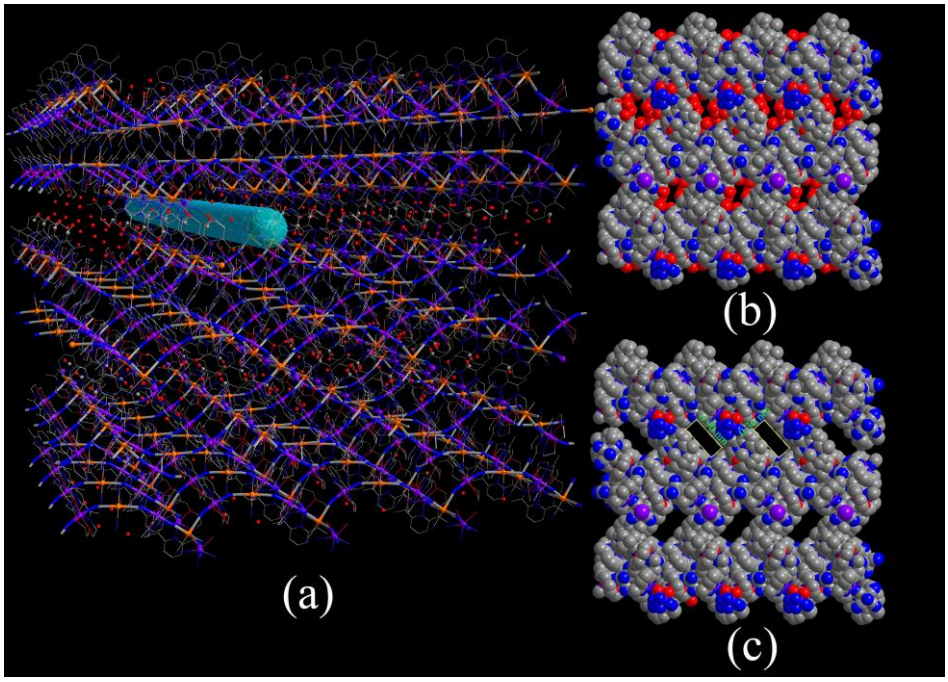

Figure S5. Some other structural graphs of **3** (a) 1D tunnel of **3**. (b) The space pilling with Vander Waals radii with solvents. (c) In absence of solvents the rectangle section measured 0.36 nm × 0.90 nm.

Table S6. Selected Bond Length [Å] and Angles [deg].

1			
Fe(1)-C(1)	1.933(9)	N(1)-C(1)-Fe(1)	176.9(8)
Fe(1)-C(2)	1.903(11)	N(2)-C(2)-Fe(1)	176.6(10)
Fe(1)-C(3)	1.924(10)	N(3)#1-C(3)-Fe(1)	179.1(10)
Fe(1)-C(4)	1.885(10)	N(4)-C(4)-Fe(1)	179.0(9)
Fe(1)-C(5)	1.944(10)	N(5)-C(5)-Fe(1)	178.6(10)
Fe(1)-C(6)	1.926(10)	N(6)#3-C(6)-Fe(1)	177.6(9)
Fe(2)-C(7)	1.945(9)	N(7)-C(7)-Fe(2)	179.0(10)
Fe(2)-C(8)	1.962(12)	N(8)-C(8)-Fe(2)	176.4(12)
Fe(2)-C(9)	1.949(10)	N(9)-C(9)-Fe(2)	176.2(8)
Fe(2)-C(10)	1.926(11)	N(10)-C(10)-Fe(2)	177.9(9)
Fe(2)-C(11)	1.898(10)	N(11)-C(11)-Fe(2)	176.9(8)
Fe(2)-C(12)	1.959(12)	N(12)-C(12)-Fe(2)	178.6(13)
Fe(3)-C(13)	1.892(9)	N(13)-C(13)-Fe(3)	175.3(9)
Fe(3)-C(14)	1.903(10)	N(14)-C(14)-Fe(3)	176.5(9)
Fe(3)-C(15)	1.931(10)	N(15)-C(15)-Fe(3)	177.4(9)
Fe(3)-C(16)	1.942(12)	N(16)-C(16)-Fe(3)	176.8(11)
Fe(3)-C(17)	1.943(10)	N(17)-C(17)-Fe(3)	178.0(8)
Fe(3)-C(18)	1.934(11)	N(18)-C(18)-Fe(3)	178.8(10)
Fe(4)-C(19)	1.904(10)	N(19)#3-C(19)-Fe(4)	177.2(11)
Fe(4)-C(20)	1.931(13)	N(20)-C(20)-Fe(4)	177.1(10)
Fe(4)-C(21)	1.919(9)	N(21)-C(21)-Fe(4)	178.6(8)
Fe(4)-C(22)	1.923(14)	N(22)-C(22)-Fe(4)	178.9(15)
Fe(4)-C(23)	1.937(12)	N(23)-C(23)-Fe(4)	177.1(9)
Fe(4)-C(24)	1.901(13)	N(24)-C(24)-Fe(4)	178.2(12)
Co(1)-O(1)	2.250(7)	C(1)-N(1)-Co(1)	148.2(7)
Co(1)-O(2)	2.298(7)	C(7)-N(7)-Co(1)	149.9(7)
Co(1)-N(1)	2.084(7)	C(9)-N(9)-Co(2)	157.3(8)
Co(1)-N(7)	2.092(7)	C(6)#2-N(6)-Co(2)	161.0(7)
Co(1)-N(25)	2.105(7)	C(11)-N(11)-Co(3)	165.8(8)
Co(1)-N(26)	2.151(9)	C(15)-N(15)-Co(3)	153.0(8)
Co(1)-N(27)	2.160(9)	C(14)-N(14)-Co(4)	156.2(9)
Co(2)-O(3)	2.299(7)	C(19)#2-N(19)-Co(4)	166.9(8)
Co(2)-O(4)	2.268(7)	C(3)#1-N(3)-Co(5)	151.9(8)
Co(2)-N(6)	2.183(8)	C(13)-N(13)-Co(5)	153.9(8)
Co(2)-N(9)	2.096(7)	C(17)-N(17)-Co(6)	150.9(7)
Co(2)-N(28)	2.147(10)	C(17)-N(21)-Co(6)	150.1(7)
Co(2)-N(29)	2.097(8)	Co(4)-N(36)	2.206(10)
Co(2)-N(30)	2.110(7)	Co(5)-O(9)	2.255(8)
Co(3)-O(5)	2.256(7)	Co(5)-N(3)	2.086(8)
Co(3)-O(6)	2.276(8)	Co(5)-N(13)	2.140(8)
Co(3)-N(11)	2.080(8)	Co(5)-N(37)	2.156(9)
Co(3)-N(15)	2.110(8)	Co(5)-N(38)	2.083(10)

Co(3)-N(32)	2.111(8)	Co(5)-N(39)	2.220(11)
Co(3)-N(33)	2.202(10)	Co(6)-O(11)	2.262(5)
Co(4)-O(7)	2.269(8)	Co(6)-O(12)	2.285(6)
Co(4)-O(8)	2.287(9)	Co(6)-N(17)	2.111(8)
Co(4)-N(14)	2.076(9)	Co(6)-N(21)	2.105(7)
Co(4)-N(19)	2.086(9)	Co(6)-N(40)	2.177(7)
Co(4)-N(34)	2.163(14)	Co(6)-N(41)	2.110(6)
Co(4)-N(35)	2.073(9)	Co(6)-N(42)	2.201(6)
#1 -x+1,-y+2,-z+1	#2 x-1,y,z	#3 x+1,y,z	

2

Fe(1)-C(1)	1.957(5)	N(1)-C(1)-Fe(1)	169.0(4)
Fe(1)-C(2)	1.947(5)	N(2)-C(2)-Fe(1)	175.4(4)
Fe(1)-C(3)	1.947(5)	N(3)#3-C(3)-Fe(1)	173.0(4)
Fe(1)-C(4)	1.929(5)	N(4)-C(4)-Fe(1)	179.5(5)
Fe(1)-C(5)	1.942(5)	N(5)-C(5)-Fe(1)	175.4(5)
Fe(1)-C(6)	1.932(5)	N(6)-C(6)-Fe(1)	174.6(5)
Co(1)-O(1)	2.243(3)	C(1)-N(1)-Co(1)	152.1(4)
Co(1)-N(1)	2.095(4)	C(2)-N(2)-Co(2)	167.2(4)
Co(1)-N(7)	2.110(5)	C(3)#2-N(3)-Co(2)	157.6(4)
Co(1)-N(8)	2.190(4)		
Co(2)-O(2)	2.290(4)	Co(2)-N(9)	2.108(4)
Co(2)-N(2)	2.081(4)	Co(2)-N(10)	2.185(5)
Co(2)-N(3)	2.092(4)	Co(2)-N(11)	2.179(4)
#1 -x,y,-z+1/2	#2 -x+1/2,y+1/2,-z+1/2	#3 -x+1/2,y-1/2,-z+1/2	

3

Fe(1)-C(1)	1.904(11)	N(1)-C(1)-Fe(1)	177.1(10)
Fe(1)-C(2)	1.922(10)	N(2)-C(2)-Fe(1)	172.8(9)
Fe(1)-C(3)	1.881(11)	N(3)-C(3)-Fe(1)	174.6(11)
Fe(1)-C(4)	1.926(10)	N(4)#3-C(4)-Fe(1)	173.3(9)
Fe(1)-C(5)	1.868(11)	N(5)-C(5)-Fe(1)	176.6(11)
Fe(1)-C(6)	1.881(10)	N(6)-C(6)-Fe(1)	179.3(12)
Fe(2)-C(7)	1.894(15)	N(7)-C(7)-Fe(2)	168.6(19)
Fe(2)-C(8)	1.893(14)	N(8)-C(8)-Fe(2)	167.5(19)
Fe(2)-C(9)	1.830(15)	N(9)-C(9)-Fe(2)	171.1(19)
Fe(2)-C(10)	1.897(16)	N(10)-C(10)-Fe(2)	167.6(18)
Fe(2)-C(11)	1.860(16)	N(11)-C(11)-Fe(2)	162.2(14)
Fe(2)-C(12)	1.885(16)	N(12)-C(12)-Fe(2)	162.7(19)
Co(1)-O(1)	2.296(11)	C(1)-N(1)-Co(1)	161.3(9)
Co(1)-O(2)	2.270(8)	C(2)-N(2)-Co(2)	159.2(9)
Co(1)-N(1)	2.080(8)	C(3)-N(3)-Co(3)	158.6(10)
Co(1)-N(8)#1	2.097(10)	C(4)#2-N(4)-Co(2)	160.3(9)
Co(1)-N(13)	2.083(15)	C(7)-N(7)-Co(3)	157.7(17)
Co(1)-N(14)	2.143(13)	C(8)-N(8)-Co(1)#4	154.2(17)
Co(1)-N(15)	2.116(13)		

Co(2)-O(3)	2.306(8)	Co(3)-O(5)	2.308(8)
Co(2)-O(4)	2.307(9)	Co(3)-O(6)	2.282(11)
Co(2)-N(2)	2.133(9)	Co(3)-N(3)	2.097(10)
Co(2)-N(4)	2.117(9)	Co(3)-N(7)	2.136(15)
Co(2)-N(16)	2.108(10)	Co(3)-N(19)	2.084(12)
Co(2)-N(17)	2.171(11)	Co(3)-N(20)	2.25(2)
Co(2)-N(18)	2.175(12)	Co(3)-N(21)	2.248(14)

#1 x,y,z-1 #2 x-1,y,z #3 x+1,y,z #4 x,y,z+1

S7. Magnetic Property Study

The temperature dependence of their susceptibilities under a 1 kOe applied field is shown in Figure 3 and 4a, the experimental $\chi_m T$ values per Co3Fe2 at 300 K are 9.0 , 8.68 and 8.79 cm^3Kmol^{-1} for **1, 2** and **3**,respectively. Presuming *g*Fe = 2.0 and a spin-only contribution was considered, get *g*Co values are equal to 2.42, 2.37 and 2.37 for them. The relative big g is owing to the considerable contribution from the orbital angular momentum of Co^{II}. For all compounds the high-temperature data obey the Curie-Weiss law, giving Weiss temperatures are 0.39, 1.62 and 2.36 K. The positive Weiss temperature values indicate dominant ferromagnetic (FO) couplings by cyanide bridged iron and cobalt ions in each compound.

For **1** and **2**, the temperature dependent $\chi_m T$ plots are going smoothly under decreasing temperatures before the rapid risings around 20 K, the maximum values (16.83 cm^3Kmol^{-1} for **1** and 14.34 cm^3Kmol^{-1} for **2**) were achieved both at 2.5 K, then they fall rapidly that may due to the strong ZFS of Co^{II} ions. According to the $\chi_m T$ values at 2.5 K, Co^{II} ions are suggested being in the low spin state, expected FO state $S_T = 3 \times 1/2 + 2 \times 1/2 = 5/2$ per Co_3Fe_2 unit, and the average g_{eff} factor for all metals are calculated to be 3.92 and 3.62 for **1** and **2** respectively. The field dependent magnetizations were measured for **1** and **2** under a temperature of 1.9 K (shown in figure 3), curves show that the magnetizations are growing fast following the increasing magnetic field, at 50 kOe the unsaturated values are 7.70 and 7.67 Nβ, and effective g for metals g_{eff} = 3.80, 3.78 for **1** and **2**.

In contrast to **2**, a relative strong inter-layer interaction is expected through its alternating closely packing in **3**. In figure 4a, **3**'s $\chi_m T$ values are increasing slowly under decreasing temperatures, a sudden rising occurs around 20 K, and the curve gets a peak (54.4 cm^3Kmol^{-1}) at 4.3 K then falls swiftly. The summit value 54.4 cm^3Kmol^{-1} is much larger than **1** and **2**, indicating a possible spontaneous magnetization at this temperature. The FCM–ZFCM curve (Figure S10a) has a sharp peak at 5.0 K, which is a feature of anti-ferromagnetic ordering, and then in lower temperature the two branches deviate from each other indicating a spontaneous magnetization below 5.0 K. In the field dependent magnetization curve at 1.9 K shown in figure S10b, the magnetization value is increasing slowly with increasing applied field, then it grows fast immediately after the field running higher than 500 Oe, the pronounced sig-mod shape indicates **3** being a meta-magnetic compound: it transfers from an anti-ferromagnetic state caused by the interlayer interaction under lower temperature and weak magnetic field to a state dominated by intra-plane Fe-Co ferromagnetic interaction at higher field. The hysteresis at higher fields looks like a thin butterfly which is also a feature of meta-magnetism, and the accurate transition filed (*Hc* = 550 Oe) was obtained by differentiating the *M* - *H* curve. An obvious hysteresis is also observed in low field

shown in the zoom-in diagram, which may be due to a long ranged week magnetic ordering, hypothetically, interlayer spin canting occurs between the AF planes, and the coercive force is about 500 Oe. This spontaneous magnetization in low temperature and low magnetic field is consistent with the phenomenon observed in FCM–ZFCM curve.

Magnetic properties of **3** are also studied in AC (alternating current) signal measurements shown in figure S11a-c, with applied field H = 0 Oe, 1000 Oe and 4000 Oe, respectively. When H = 0, both real and imaginary parts have signals and peaks. The real peaks appear at T = 5.0 K, this is corresponding to its FCM–ZFCM curve, indicating an AF ordering, and the frequency dependent imaginary peaks appears below 4.5 K indicating a spontaneous magnetization caused by spin canted. When H = 1000 Oe, the real part signals get weaker, but the imaginary part signals get stronger, and double peaks have been observed in both two parts with frequency dependence to certain extents. The two peaks (real and imaginary parts) appear in lower temperature are corresponding to a week ferromagnetic order in an apply field of 1000 Oe, the two peaks in higher temperature zone are caused by another order state originated from intra-layer Fe Co interactions and spontaneous magnetization occurs. So when applied with a magnetic field of 1000 Oe, the material experience transition from a week ferromagnetic state caused by inter-layer spin canted to another ordering state by intra-layer magnetic exchanging with an increasing temperature. Peaks appear at specific positions of these two states, respectively.

When the applied field increasing as high as 4000 Oe, the peaks at lower temperatures disappear, the remaining singles in higher temperatures are still frequency dependent and get weaker, both peaks in real and imaginary parties are moving towards higher temperature zone. These phenomena indicate that the compound is keeping one ferromagnetic state through this measurement.

In order to understand these information easily, we draw a magnetic phase diagram of compound **3** very qualitatively (Figure S11d). transition filed (Hc = 550 Oe) is obtained by differentiating the field dependent magnetization curve measured at T = 1.9 K should be the border of antiferromagnetic and ferromagnetic zones, but at lower temperatures, transition temperature to week ferromagnetic state is higher than 550 Oe, this conclusion can be deduced by the following facts: 1) Differentiating the temperature dependent $\chi_m T$–T curve (Figure 4a) measured in a applied field of 1000 Oe, which is higher than the transition field, a obvious inverted peak (at T = 4.9 K) exists and indicates a phase transition at this temperature; 2) the $\chi_m T$–T measurement under the applied field of 1000 Oe get to a peak of 54.4 cm^3Kmol^{-1} at 4.3 K, the value is more higher **1** and **2**, which indicates **3** is of a long ranged ordering state caused by inter-layer spin canted at the temperature of 4.3 K.

Three AC measurements are experiencing three different courses represented by different arrows shown in figure S11d. When applied with field of zero (3 Oe actually), the unique peak in real part is corresponding to the FC-ZFC measurement shown in Figure 7b, the peak in imaginary part is related to the spontaneous magnetization of spin canted state; at the applied field of 1000 Oe, the measurement experienced two spontaneous magnetization zones, the double peaks both in real and imaginary parts are their properties of two states themselves; the inter-layer exchanges are broken in the applied field of 4000 Oe, so only intra-layer ferromagnetic properties were detected.

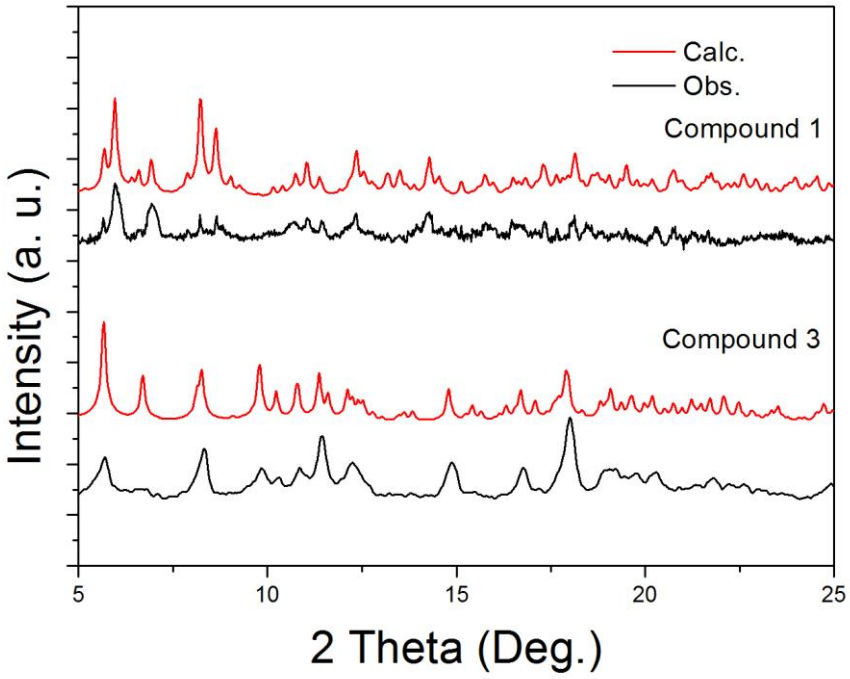

Figure S8. Simulated and measured PXRD patterns for **1** and **3**. Analysis for **2** was absent for its instability in room temperature. The accidental extinctions of some peaks may be related to the details of samples' grinding or disordered solvents in room temperature.

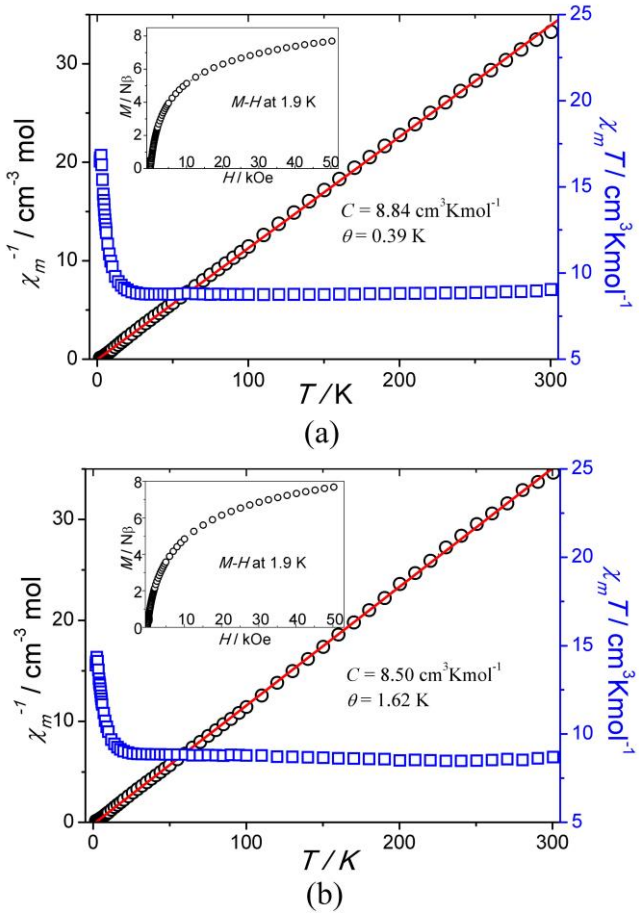

Figure S9: Magnetic measurement of a) 1 and b) 2: Temperature dependent $\chi_m T$ plot and Curie-Weiss fitting $1/\chi_m$ vs T, field dependent magnetization in inner pictures.

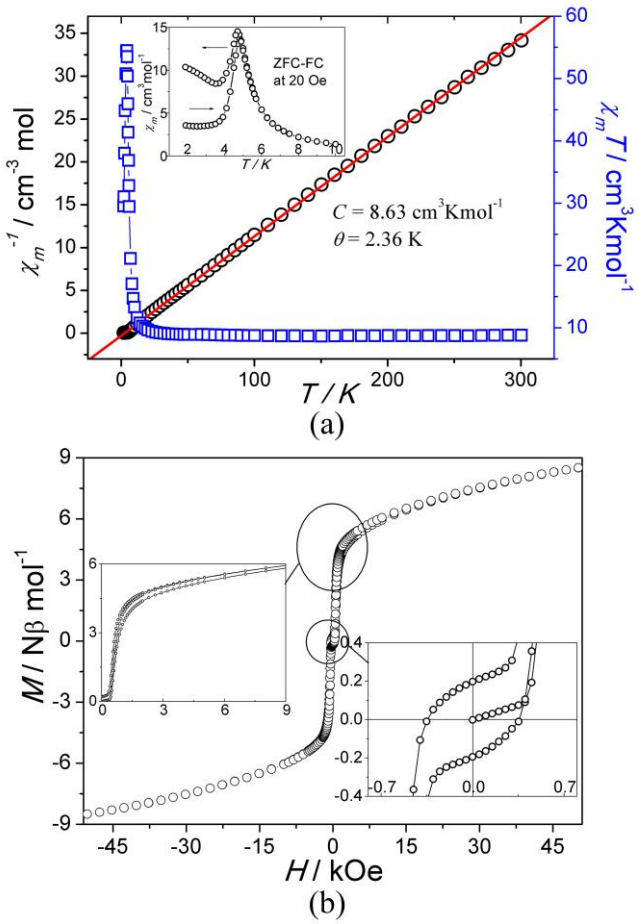

Figure S10: Magnetic measurement of compound **3**. a) Temperature dependent $\chi_m T$ plot and the Curie-Weiss fitting; inner picture shows a FCM–ZFCM measurement at the applied field of 20 Oe.

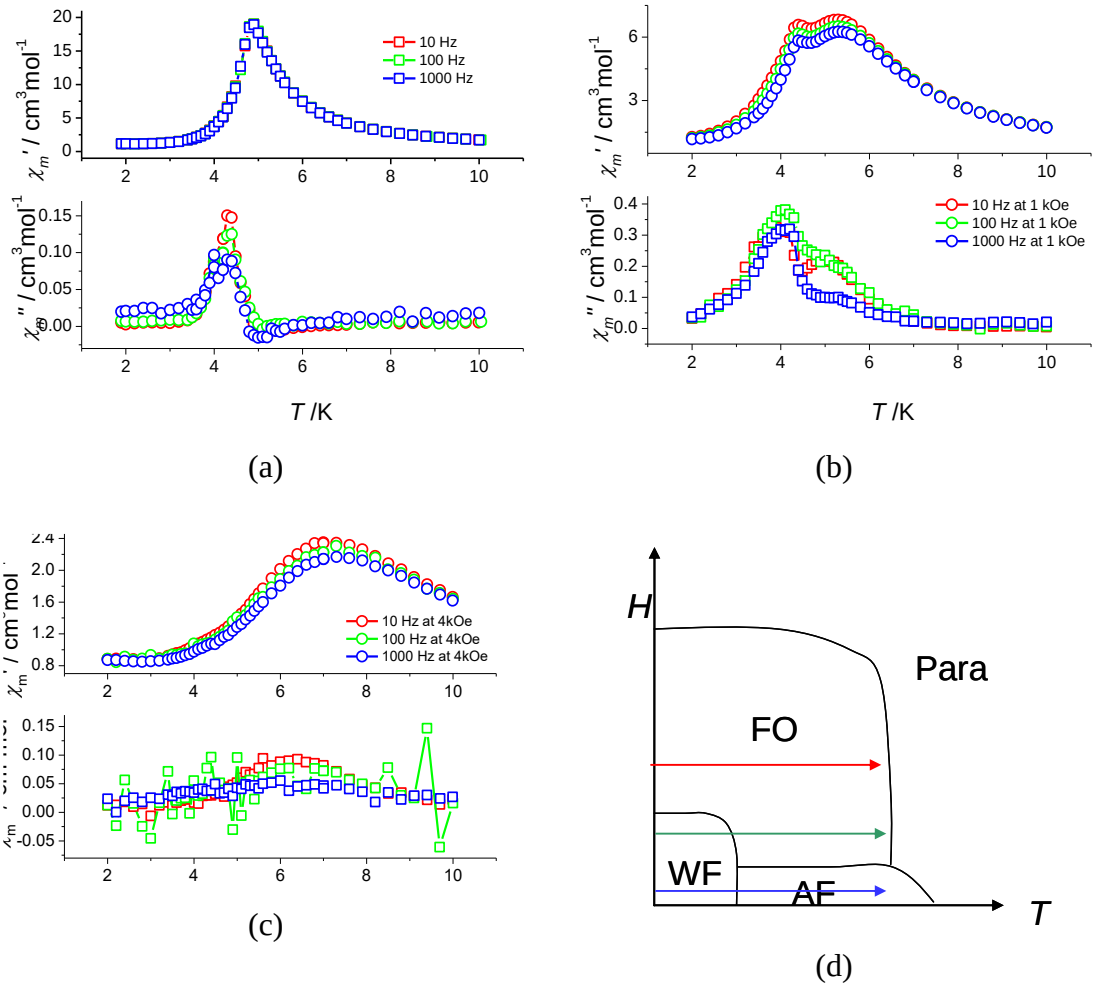

Figure S11. The alternating currency measurement under a applied field of (a) 0 Oe (b) 1000 Oe (b) 4000 Oe, and schematic magnetic phase diagram of **3** (d).

Reference

1. Spek A L. PLATON SQUEEZE: a tool for the calculation of the disordered solvent contribution to the calculated structure factors[J]. *Acta Crystallographica Section C: Structural Chemistry*, **2015**, 71(1): 9-18.
2. Mulay L N, Boudreaux E A. Theory and applications of molecular diamagnetism [M]. Wiley, **1976**.